

PCCP

Accepted Manuscript



This is an *Accepted Manuscript*, which has been through the Royal Society of Chemistry peer review process and has been accepted for publication.

Accepted Manuscripts are published online shortly after acceptance, before technical editing, formatting and proof reading. Using this free service, authors can make their results available to the community, in citable form, before we publish the edited article. We will replace this *Accepted Manuscript* with the edited and formatted *Advance Article* as soon as it is available.

You can find more information about *Accepted Manuscripts* in the [Information for Authors](#).

Please note that technical editing may introduce minor changes to the text and/or graphics, which may alter content. The journal's standard [Terms & Conditions](#) and the [Ethical guidelines](#) still apply. In no event shall the Royal Society of Chemistry be held responsible for any errors or omissions in this *Accepted Manuscript* or any consequences arising from the use of any information it contains.

**Fabrication of a novel $\text{Ag}_3\text{VO}_4/\text{WO}_3$ heterojunction with
enhanced visible light efficiency in photocatalytic
degradation of TC**

Ming Yan^a, Yilin Wu^b, Fangfang Zhu^b, Yinqun Hua^a, Weidong Shi^{b,}*

*^a School of Material Science and Engineering, Jiangsu University, Zhenjiang 212013,
China*

*^b School of Chemistry and Chemical Engineering, Jiangsu University, Zhenjiang
212013, China*

*Corresponding Author**

E-mail: shiweidong321123@163.com

Telephone Number: +86-511-88791800; fax: +86 0511-88791800

Abstract: The constructing of efficient photocatalysts for environmental remediation has attracted a great deal of attention in recent years. In this study, the novel $\text{Ag}_3\text{VO}_4/\text{WO}_3$ heterojunction photocatalyst has been successfully prepared via a hydrothermal process and a facile precipitation reaction. Under visible light irradiation, the hybrid materials could significantly enhance photocatalytic activity for the degradation of tetracycline (TC) in comparison with the single Ag_3VO_4 and WO_3 . Within 30min, 71.2% TC could be photodegraded by the optimum sample (10%A/W), which was about 3.1 times and 4.6 times higher than that of the individual Ag_3VO_4 and WO_3 , respectively. On the basis of the active species trapping experiments and ESR, the photocatalytic oxidation mechanism of $\text{Ag}_3\text{VO}_4/\text{WO}_3$ composite was also discussed. It can be assumed that the enhancement of the photocatalytic activity was attributed to the heterojunction which could widely accelerate the photogenerated electron-hole pair's separation. In general, the WO_3 hybridized with Ag_3VO_4 will also efficiently address the problem of low photocatalytic activity.

Key words: $\text{Ag}_3\text{VO}_4/\text{WO}_3$, heterojunction, tetracycline, visible light

Introduction

In recent times, the abuse of antibiotics in the field of pharmaceutical has generated serious threats to ecosystem and human health [1, 2]. As a very noted broad-spectrum antibacterial agent, tetracycline (TC) antibiotics are widely used in human medicine, livestock, and the treatment of bacterial infection, which are usually detected in aquatic environments. Therefore, it is indispensable to remove TC from aqueous environments. Unfortunately, the traditional treatments are often limited by the high cost and low efficiency [3, 4]. Recently, as an efficient yet green technology, photocatalysis oxidation has been regarded as a significant and predominant pathway to resolve the increasing energy and environmental crisis [5-10] and offered a better tool for transforming and degrading the pollutants [11-13]. In a view of energy conversion, visible light counts for more than 43% of the incoming solar energy. Thus, development of a high-efficiency visible-light-driven photocatalyst for the photodegradation of TC is urgently needed [14-16].

Tungsten trioxide (WO_3), a transition metal oxide semiconductor, has been considered as an effective candidate for pollutant degradation due to its narrow band gap (2.6-2.8 eV), nontoxicity and resilience to photocorrosion [17-20]. In addition, as a promising visible-light-driven photocatalyst, WO_3 has also been reported for oxygen evolution [21-22]. However, the efficiency of the single-phase WO_3 is still confined by fast recombination of photo-generated charge carriers, leading to the low photocatalytic performance [23-24]. Over the past years, numerous efforts have been devoted to improve the photocatalytic activity of the single-phase semiconductor, such as metallic or nonmetallic element-doping [25], coupling with other semiconductors [26-27] and so on. As is well known, the construction of heterojunction structure is a very efficient route to overcome this defect [28-29] by realizing the interfacial charge transfer between semiconductors,

such as coupling with the wide-band gap semiconductors (WO_3/TiO_2 [30] and WO_3/ZnO [31] etc) or the narrow-band gap semiconductors ($\text{WO}_3/\text{g-C}_3\text{N}_4$ [32] and WO_3/CdS [33] etc), thus inhibiting the recombination of photogenerated electrons and holes. However, compared to the WO_3 -based composites with wide-band gap semiconductors, the narrow-band gap photocatalyst can not only largely improve the optical absorption property, but also enhance their solar energy conversion. Thus far, the construction of WO_3 -based heterojunction system with narrow band gap semiconductor photocatalyst for efficiently utilizing the solar light is still facing the challenge.

Importantly, since pioneering contributions by the research group from Kouta [34], the monoclinic-scheelite Silver Vanadate (Ag_3VO_4), a visible-light-driven photocatalyst with the narrow gap (2 eV), has been of considerable interest and extensively developed because of its good performance for water splitting into H_2 and O_2 . However, to the best of our knowledge, WO_3 hybridized with Ag_3VO_4 about photocatalytic performance for pollution degradation have not been reported.

Herein, we have, for the first time, reported a novel $\text{Ag}_3\text{VO}_4/\text{WO}_3$ heterojunction by developing a two-step hydrothermal and precipitating methodology. The photocatalytic activity was evaluated by the degradation of TC under visible light irradiation ($\lambda \geq 420\text{nm}$). The as-prepared heterojunction materials showed enhanced photocatalytic performance in comparison with the pure WO_3 and Ag_3VO_4 . Furthermore, tentative mechanism was also discussed based on the active species trapping experiments and electron spin resonance (ESR) analysis.

2. Experiment

2.1. Chemicals

Sodium tungsten oxide ($\text{Na}_2\text{WO}_4 \cdot 2\text{H}_2\text{O}$), silver nitrate (AgNO_3), sodium orthovanadate

(Na_3VO_4) were purchased from Aladdin (China). Nitric acid (HNO_3) and tetracycline (TC) were purchased from Sinopharm (China). All chemicals were of analytical reagent grade and used without further purification, deionized water was used in all experiments.

2.2. Synthesis of the WO_3

WO_3 nanosheets were synthesized via a hydrothermal process. Typically, 65% nitric acid (10 ml) was immersed dropwise into 50 mL of deionized water with stirring for 10 min. Then 20 mL $\text{Na}_2\text{WO}_4 \cdot 2\text{H}_2\text{O}$ solution (containing 3 mmol $\text{Na}_2\text{WO}_4 \cdot 2\text{H}_2\text{O}$) and nitric acid were mixed together to form the light yellow solution. After stirring for another 1h, the obtained precursor was transferred into a Teflon-lined stainless steel of 100 mL capacity, which was carried out at 180°C for 3 h. When the container cooled down to the room temperature, the final yellow products were collected by centrifugation, washed with the deionized water and ethanol for three times, dried at 60°C for 12 h.

2.3. Synthesis of $\text{Ag}_3\text{VO}_4/\text{WO}_3$

The $\text{Ag}_3\text{VO}_4/\text{WO}_3$ samples were prepared by a simple in-situ deposition method. Briefly, a certain amount of WO_3 samples (2.5, 3.3, 5 and 10 mmol) were dissolved in 50 mL deionized water. Then, 1.5 mmol AgNO_3 was added into the above solution under vigorous stirring for 30 min. Subsequently, 50 mL aqueous solution (containing 0.5 mmol Na_3VO_4) was added dropwise to the above solution and kept stirring violently for 7 h in the darkness. Lastly, the obtained $\text{Ag}_3\text{VO}_4/\text{WO}_3$ hybrid photocatalysts at different mole percent ratio (abbreviated as 5% A/W, 10% A/W, 15% A/W and 20% A/W) were centrifuged and washed with deionized water and ethyl alcohol, dried in vacuum at 60°C for 12 h. For comparison, bare Ag_3VO_4 was prepared similarly but without adding the as-prepared WO_3 sample.

2.4. Characterization

The phases and crystal structures of the as-prepared products were investigated by X-ray diffraction (XRD) patterns with a D/MAX-2500 diffract meter (Rigaku, Japan) equipped with a nickel-filtered Cu K α radiation source ($\lambda = 1.54056\text{\AA}$). The morphology of the samples were observed by scanning electron microscopy (SEM) using a Hitachi S-4800 field emission SEM (FESEM, Hitachi, Japan). Transmission electron microscopy (TEM) and high-resolution transmission electron microscopy (HRTEM) were gathered on an F20 S-TWIN electron microscope (Tecnai G2, FEI Co.), using a 200kV accelerating voltage. X-ray photo-electron spectroscopy (XPS) was conducted on a PHI5000 Versa Probe electron spectrometer using Al K α radiation (ULVAC-PHI, Japan), identifying surface chemical composition and chemical states of the catalysts. The UV-vis diffuse reflectance spectra (DRS) were measured using a spectrophotometer (Shimadzu UV2550), BaSO₄ was used as a reflectance standard. To detect the generation of activated species, Electron Spin Resonance (ESR) analysis was conducted with a Bruker EPR JES-FA200 spectrometer. The electrochemical impedance spectroscopy (EIS) was measured with an electrochemical analyzer (CHI 660B Chenhua Instrument Company).

2.5. Photocatalytic Degradation of TC

The photocatalytic degradation action of TC was carried out at 308 K in a photochemical reactor under the irradiation of visible light. In the typical process, 50 mg as-prepared samples were added into the 100 mL solution of TC (10 mg/L), prior to irradiation, the suspensions were kept stirring for 30 min in darkness to insure the adsorption equilibrium. The photochemical reactor was irradiated with a 300 W xenon lamp. UV light with a wavelength less than 420 nm was removed by a UV-cutoff filter. In 5 min irradiation intervals, a battery of aqueous solution

samples (6 mL) were collected and separated from the suspended catalyst particles for analysis.

The photocatalytic degradation ratio (DR) was calculated via the following formula:

$$DR = (1 - A_i / A_0) \times 100\% \quad (1)$$

where A_0 is the foremost absorbency of TC that arrived adsorption equilibrium, A_i is the absorbency after the sampling analysis. The concentration of TC was measured on a UV-vis spectrophotometer at its maximum absorption wavelength (357 nm).

3. Results and Discussion

3.1. Structure and morphology

Fig. 1 shows the XRD patterns for the WO_3 , $\text{Ag}_3\text{VO}_4/\text{WO}_3$ hybrid materials, and pure Ag_3VO_4 . As can be seen from the picture, the nanosheet structure WO_3 was in good agreement with the monoclinic phase of WO_3 in the JCPDS card (JCPDS No.43-1035), while the diffraction peaks of Ag_3VO_4 matched with its monoclinic phase (JCPDS No.43-0542). For the $\text{Ag}_3\text{VO}_4/\text{WO}_3$ composites, the characteristic peaks of WO_3 were predominant, whereas the intensities of Ag_3VO_4 peaks became stronger as increasing the content of Ag_3VO_4 . In addition, we can't discover any other impurity phases, indicating that the as-prepared $\text{Ag}_3\text{VO}_4/\text{WO}_3$ heterostructured photocatalysts were two-phase hybrid.

The morphology was obtained by SEM. From the Fig. 2a, it can be observed that the pure WO_3 was composed of square sheet-like structures, and the Fig. 2b exhibit the thickness of the sheet structure was about 30 nm. The as-prepared Ag_3VO_4 was mainly composed of irregular spherical nanoparticles in the Fig. 2c. After introducing the Ag_3VO_4 on the surface of the WO_3 in the Fig. 2d, some nanoparticles appeared on the square sheet-like structure, resulting in the formation of the heterostructure.

Further insight into the morphology and detailed surface nature of the $\text{Ag}_3\text{VO}_4/\text{WO}_3$ composites were characterized by the TEM and HRTEM. Fig. 2e offers an over-view image of the TEM. It clearly display that the Ag_3VO_4 nanoparticles dispersed over the surface of WO_3 nanosheets. The lattice interlinear spacing (Fig. 2f) of $d=0.277$ nm and $d=0.262$ nm were coincided with the (121) plane of Ag_3VO_4 and the (202) plane of WO_3 respectively, which clearly suggested that the composites between WO_3 and Ag_3VO_4 have been formed.

3.2. XPS analysis

The chemical states of the as-prepared 10%A/W sample were examined by the XPS analysis, the results of which were displayed in the Fig. 3a. According to the XPS observations, the peaks of Ag, W, V, O and C were all detected in the 10%A/W sample. The C 1s peak located at 284.6 eV can be attributed to the signal from carbon contained in the instrument and was used for calibration [35-37]. Fig. 3b exhibits two strong peaks at 367.9 eV and 374.1 eV, which were assigned to Ag $3d_{5/2}$ and Ag $3d_{3/2}$, respectively, verifying that the Ag^+ cations originate from Ag_3VO_4 . No peak was observed at 369.2 eV or 375.8 eV, indicating that no Ag^0 was formed during the preparation [38]. In the high resolution spectrum of W 4f (Fig. 3c), there were two peaks at 35.37 eV and 37.62 eV, which corresponded to the W $4f_{7/2}$ and W $4f_{5/2}$. The bands were attributed to W^{6+} . In the V 2p and O 1s high-resolution XPS spectrum in the Fig. 3d, the V 2p peak at 517.2eV and the O 1s peak at 531.1 eV, corresponding to V^{5+} as well as O^{2-} in the 10%A/W sample. The results of the XPS analysis were consistent with those of the XRD analysis, further confirming the coexistence of Ag_3VO_4 and WO_3 in the composite powders.

3.3. UV-vis absorption spectra

Fig. 4a displays the UV-vis diffuse reflectance spectroscopy of the as-prepared samples.

According to the spectra, the pure Ag_3VO_4 presented a light absorption edge at about 600 nm, while the WO_3 sample showed a light absorption edge at 460 nm. Meanwhile, the absorption edges of the $\text{Ag}_3\text{VO}_4/\text{WO}_3$ composites with different mole percent ratio somehow changed in an orderly pattern and possess visible light response. Energy band gaps (E_g) of different samples can be calculated with the following equation [39]:

$$\alpha h\nu = A (h\nu - E_g)^{n/2} \quad (2)$$

where α , h , ν , A , E_g are the absorption coefficient, Planck's constant, the incident light frequency, constant and the band gap energy, respectively. What is more, n depends on the transition type of semiconductor. The $n=1$ for direct transition, while n is 4 for indirect transition. Therefore, the values of Ag_3VO_4 and WO_3 are 1 and 4, respectively [33, 40]. According to the Fig. 4b, the energy band gaps of WO_3 and Ag_3VO_4 from the plots of $(\alpha h\nu)^2$ versus $h\nu$ can be estimated were 2.7 eV and 2 eV. With increasing the content of Ag_3VO_4 , the E_g of the $\text{Ag}_3\text{VO}_4/\text{WO}_3$ composite was closer to that of the Ag_3VO_4 .

3.4. Photocatalytic activity

The photocatalytic activity of the as-prepared $\text{Ag}_3\text{VO}_4/\text{WO}_3$ samples were evaluated by the degradation of TC under visible light irradiation ($\lambda > 420$ nm). For comparison, the single WO_3 and Ag_3VO_4 were also provided. As shown in the Fig. 5a, pure WO_3 and bare Ag_3VO_4 exhibited low photocatalytic performance, however, the photocatalytic activity can be efficiently enhanced after introducing appropriate amount of Ag_3VO_4 in the WO_3 . Among all the samples, the 10%A/W sample displayed the highest photocatalytic performance. Within 30 min irradiation, about 71.2% of TC was degraded. Nevertheless, the content of Ag_3VO_4 has a significant influence on photocatalytic activity, when the molar percent ratio exceed 10%, the photocatalytic efficiency

declined but was still higher than that of the pure WO_3 and Ag_3VO_4 . Such an optimal synergistic effect between WO_3 and the other semiconductors had been widely observed in previous works [32]. Fig. 5b displays temporal evolution of the UV-vis spectral variations during the TC degradation over 10%A/W sample under visible light irradiation. Obviously, the main absorption peak of TC molecule located at 357 nm, which decreased rapidly with extension of the exposure time.

The kinetic behavior was employed to further investigate the photodegradation of TC. As can be seen in the Fig. 5c, the plots of TC decomposition matched the pseudo-first order kinetic correlation:

$$\ln(C_0/C) = k_{\text{app}} t \quad (3)$$

where C and C_0 are the TC concentration at irradiation time of t and the initial concentration at $t=0$, respectively. K_{app} represents the degradation apparent rate constant. The k values of different samples were exhibited in the Fig. 5d. Obviously, the highest value of k is 0.03938 for 10%A/W, which is consistent with the result of photocatalytic degradation.

3.5 The intermediates of TC degradation

It is significant to report the intermediates of TC by the LC-MS, the results were displayed in the Fig. 6. From the Fig. 6a, it can be clearly found that the m/z of the major peak is at the value of 445, corresponding to TC. From the analysis of LC-MS, as the major reactive species h^+ attacked the TC. The successive ions fragmentation during collision-induced dissociation is in the following order: $m/z=445 \rightarrow m/z=406$ (by loss of OH, H and CH_3) $\rightarrow m/z=362$ (by loss of CONH_2) $\rightarrow m/z=318$ (by loss of N, CH_2 and CH_3) $\rightarrow m/z=$ (then by loss of CH, C, H and OH). Based on the conclusion of the experimental and the reported studies [41], the possible processes

of the degradation were shown in Fig. 7. At last, the intermediate products would be degraded to the small inorganic molecular material.

3.6. Electrochemical impedance spectroscopy

Electrochemical impedance spectroscopy (EIS) was finally carried out to explore the process of their charge transfer resistance of pure WO_3 , Ag_3VO_4 and 10%A/W samples. The radius of the arc about the EIS Nyquist plot represent the charge transfer rate occurring at the contact interface between the working electrode and electrolyte solution. The smaller radius of the Nyquist circle represents the lower charge-transfer resistance. As can be seen from the Fig. 8a, the arc radius on EIS of the 10%A/W sample was smaller than that of the bare WO_3 and Ag_3VO_4 , indicating that the 10%A/W sample presented the lowest resistance, which could accelerate the photogenerated electron-hole pair's separation, improving the separation efficiency.

3.7. Mechanism

A series of active species trapping experiments for the TC degradation over the 10%A/W sample were carried out to explore the photocatalytic mechanism. In the Fig. 8b, when the triethanolamine (TEA) [42-44] was added into reaction solution to trap the holes (h^+), the photodegradation ratio was significantly declined (23.4%) compared to the reaction without TEA, indicating that h^+ play major role during the progress of photodegradation. As iso-propanol (IPA) [45] for $\bullet\text{OH}$ was added, the photodegradation was inhibited (58.1%), suggesting the $\bullet\text{OH}$ also plays an important role in the photocatalytic process. However, the photocatalytic degradation ratio (82.5%) of TC was obviously increasing with the addition of AgNO_3 for e^- [42-44], indicating that the scavenger of e^- had less opportunity for electron-hole pairs' recombination and facilitated the production of more holes to participate in redox reaction. The results were consistent with the ideas we proposed, further demonstrating the $\bullet\text{OH}$ and h^+ do exist in the process of TC degradation.

The electron spin resonance (ESR) technique was further used to explore the reactive species evolved during the photocatalytic reaction process. Before to determine the reactive species, 10 mg samples were dissolved in 0.5 mL deionized water, and then 30 μ L 5,5-dimethyl-1-pyrroline N-oxide (DMPO) was added with ultrasonic dispersion for 5 min. The 10%A/W hybrid materials suspension are irradiated for 8 min by a Quanta-Ray Nd:YAG pulsed laser system. From the Fig. 8c, it can be observed that no ESR signals were exhibited as the reaction was carried out in the darkness. On the contrary, four characteristic peaks with the intensity of 1:2:2:1 were observed under visible light irradiation. The characteristic peak intensity of 1:2:2:1 is the evidence that OH• radicals were indeed formed on the 10% A/W sample. From the result of ESR, we concluded that certain visible light irradiation was essential to the generation of •OH radical and it was confirmed that •OH was produced on the surface of the 10%A/W composites.

In order to explain the photocatalytic reaction mechanism, we carried out band position calculations by a plain method as the literature reported with the following equation [46]:

$$E_{CB} = X - E^e - 1/2 E_g \quad (4)$$

$$E_{CB} = E_{VB} - E_g \quad (5)$$

where E_{CB} and E_{VB} are the conduction band and valence band edge potentials, respectively; X is the electronegativity of the semiconductor (Ag_3VO_4 is 5.645 eV and WO_3 is 6.49 eV [46, 32]); E^e is the energy of free electrons on the hydrogen scale (4.5 eV); and E_g is the band gap energy of the semiconductor. According to the calculation, the E_{CB} of the Ag_3VO_4 and WO_3 were 0.145 eV and 0.64 eV respectively, and the E_{VB} were estimated to be 2.145 eV and 3.34 eV, respectively.

Based on the active species trapping experiments, ESR and calculated energy bands, a possible photocatalytic mechanism of Ag_3VO_4/WO_3 heterojunction was proposed in the Fig. 8d. When the

$\text{Ag}_3\text{VO}_4/\text{WO}_3$ sample subjected to visible light irradiation with photon energy higher or equal to the band gaps of Ag_3VO_4 and WO_3 , electrons can be excited from the VB to the CB with simultaneous generation of holes in the VB. Due to the CB of Ag_3VO_4 is more negative than that of the WO_3 , electrons on the CB of Ag_3VO_4 can be easily injected into the CB of WO_3 by the interface. Simultaneously, the VB edge level of WO_3 is more positive than that of the Ag_3VO_4 , holes in the VB edge of the WO_3 will transfer to that of the Ag_3VO_4 , which effectively inhibited recombination and improved the separation of photogenerated electrons and hole. After the migration of the photo-induced carriers, the photo-induced and transferred electrons in the CB of WO_3 . According to the calculation, the CB of WO_3 is 0.64 eV, the $\cdot\text{O}_2^-$ could not be produced because of more positive reduction potential of -0.33 eV/NHE ($\text{O}_2/\cdot\text{O}_2^-$) by electrons [47]. However, due to the reduction potential of $\text{O}_2/\text{H}_2\text{O}_2$ was 0.695 eV, the electrons can react with O_2 and H^+ to generate $\cdot\text{OH}$ by the following way: $\text{O}_2 + 2\text{e}^- + 2\text{H}^+ = \text{H}_2\text{O}_2$, $\text{H}_2\text{O}_2 + \text{e}^- = \cdot\text{OH} + \text{OH}^-$ [48]. On the contrary, the h^+ transfer to the valence band of the Ag_3VO_4 . Compared with the potential of $\cdot\text{OH}/\text{OH}^-$ (2.38 eV/NHE) and $\cdot\text{OH}/\text{H}_2\text{O}$ (2.72 eV/NHE) [42], the VB of Ag_3VO_4 ($E_{\text{VB}} = 2.14$ eV) is more negative, so the $\cdot\text{OH}$ could not produce with the react of h^+ , OH^- and H_2O . The h^+ can just react with TC, immediately.

4. Conclusion

In summary, we have first successfully proposed a facile yet efficient $\text{Ag}_3\text{VO}_4/\text{WO}_3$ heterojunction photocatalyst by developing a two-step hydrothermal and precipitating reaction. The as-prepared hybrid materials showed much higher photocatalytic activity for the TC degradation than that of the single semiconductor, and the optimized photocatalytic efficiency was 71.2% remove ratio of TC in 30 min. This largely enhanced photocatalytic activity has been

successfully obtained due to the formation of the heterojunction, which would widely improve the separation performance and prolonged the lifetime of the photogenerated charge carriers. Meanwhile, the WO_3 hybridized with Ag_3VO_4 could also solve the problem of low photocatalytic performance. Finally, we envision that the as-prepared $\text{Ag}_3\text{VO}_4/\text{WO}_3$ will provide a promising approach for water purification application and environmental remediation.

Acknowledgements:

This work was financially supported by the National Natural Science Foundation of China (21276116, 21477050, 21301076 and 21303074), Excellent Youth Foundation of Jiangsu Scientific Committee (BK20140011), Chinese-German Cooperation Research Project (GZ1091), Program for High-Level Innovative and Entrepreneurial Talents in Jiangsu Province, Program for New Century Excellent Talents in University (NCET -13-0835), Henry Fok Education Foundation (141068) and Six Talents Peak Project in Jiangsu Province (XCL-025).

References:

- [1] M. D. Hernando, S. De Vettori, M. J. Martinez Bueno, A. R. Fernandez-Alba, *Chemosphere*, 2007, 68, 724.
- [2] R. Jain, M. Mathur, S. Sikarwar, A. Mittal, *Journal of Environment Management*. 2007, 85, 956.
- [3] O. Hamdaoui, *Desalination*, 2011, 271, 279.
- [4] W. L. Zhang, Y. Li, C. Wang, P. F. Wang, *Desalination*, 2011, 266, 40.
- [5] M. R. Hoffmann, S. T. Martin, W. Choi, D. W. Bahnemann, *Chem.Rev*, 1995, 95, 69.

- [6] H. Lee, J. Choi, S. Lee, S. T. Yun, C. Lee, J. Lee, *Appl. Catal. B.*, 2013, 138, 311.
- [7] S. A. Singh, G. Madras, *Sep. Purif. Technol.*, 2013, 105, 79.
- [8] H. Katsumata, Y. Oda, S. Kaneco, T. Suzuki, *RSC Adv.*, 2013, 3, 5028.
- [9] C. C. Pei, W. W. Leung, *Sep. Purif. Technol.*, 2013, 114, 108.
- [10] Y. Jiang, R. Amal, *Appl. Catal. B.*, 2013, 138, 260.
- [11] N. Wetchakun, S. Chaiwichain, B. Inceesungvorn, K. Pingmuang, S. Phanichphant, A. I. Minett, J. Chen, *Appl. Mater. Interfaces*, 2012, 4, 3718.
- [12] H. P. Li, J. G. Liu, W. G. Hou, N. Du, R. J. Zhang, X. T. Tao, *Appl. Catal. B.*, 2014, 160, 89.
- [13] T. Wang, C. J. Li, J. Y. Ji, Y. J. Wei, P. Zhang, S. P. Wang, X. B. Fan, *ACS Sustainable Chem. Eng.*, 2014, 2, 2253.
- [14] J. Jeong, W. Song, W. J. Cooper, J. Jung, J. Greaves, *Chemosphere*, 2010, 78, 533.
- [15] X. B. Chen, S. H. Shen, L. J. Guo, S. S. Mao, *Chem. Rev.*, 2010, 110, 6503.
- [16] P. W. Huo, Z. Y. Lu, X. L. Liu, X. Gao, J. M. Pan, D. Wu, J. Ying, H. M. Li, Y. S. Yan, *Chem. Eng. J.*, 2012, 198, 73.
- [17] X. T. Su, F. Xiao, Y. N. Li, J. K. Jian, Q. J. Sun, J. D. Wang, *Mater. Lett.*, 2010, 64, 1232.
- [18] P. Q. Wang, Y. Bai, P. Y. Luo, J. Y. Liu, *Catal. Commun.*, 2013, 38, 82.
- [19] X. Zhang, X. Lu, Y. Shen, J. Han, L. Yuan, L. Gong, Z. Xu, X. Bai, M. Wei, Y. Tong, Y. Gao, J. Chen, J. Zhou, Z. L. Wang, *Chem. Commun.*, 2011, 47, 5804.
- [20] Q. Xiang, G. F. Meng, H. B. Zhao, Y. Zhang, H. Li, W. J. Ma, J. Q. Xu, *J. Phys. Chem. C.*, 2010, 114, 2049.

- [21] Y. P. Xie, G. Liu, L. Yin, H. M. Cheng, *J. Mater. Chem.*, 2012, 22, 6746.
- [22] J. Huang, L. Xiao, X. Yang, *Mater. Res. Bull.*, 2013, 48, 2782.
- [23] T. Arai, M. Horiguchi, M. Yanagida, T. Gunji, H. Sugihara, K. Sayama, *Chem. Commun.*, 2008, 5565.
- [24] B. Weng, J. Wu, N. Zhang, Y. J. Xu, *Langmuir*; 2014, 30, 5574.
- [25] N. Jacob, G. Madras, N. Kottam, T. Thomas, *Industrial & Engineering Chemistry Research*, 2014, 53, 5895-5904.
- [26] F. X. Cheng, H. N. Wang, X. P. Dong, *Chemical Communications*, 2015, 51, 7176-7179.
- [27] L. Huang, F. Peng, H. J. Wang, H. Yu, Z. Li, *Catalysis Communications*, 2009, 10, 1839-1843.
- [28] T. Arai, M. Yanagida, Y. Konishi, Y. Iwasaki, H. Sugihara, K. Sayama, *J. Phys. Chem. C*, 2007, 111, 7574.
- [29] H. Widiyandari, A. Purwanto, R. Balgis, T. Ogi, K. Okuyama, *Chem. Eng. J.*, 2012, 180, 323.
- [30] K. R. Reyes-Gil, Z. D. Stephens, V. Stavila, D. B. Robinson, *ACS Appl. Mater. Interfaces*, 2015, 7, 2202.
- [31] S. Adhikari, D. Sarkar, G. Madras, *RSC Adv.*, 2015, 5, 11895.
- [32] S. F. Chen, Y. F. Hu, S. G. Meng, X. L. Fu, *Appl. Catal. B*, 2014, 150, 564.
- [33] L. J. Zhang, S. Li, B. K. Liu, D. J. Wang, T. F. Xie, *ACS Catal.*, 2014, 4, 3724.
- [34] N. Boonprakob, N. Wetchakun, S. Phanichphant, D. Waxler, P. Sherrell, A. Nattestad, J. Chen, B. Inceesungvorn, *Colloid Interface Sci.*, 2014, 417, 402.
- [35] J. Su, X. X. Zou, G. D. Li, X. Wei, C. Yan, Y. N. Wang, J. Zhao, L. J. Zhou, J. S. Chen, *J. Phys. Chem. C*, 2011, 115, 8064.

- [36] H. Q. Wang, Z. B. Wu, Y. Liu, *J. Phys. Chem. C*, 2009, 113, 13317.
- [37] J. Zhang, J. X. Xia, S. Yin, H. M. Li, H. Xu, M. Q. He, L. Y. Huang, Q. Zhang, *Colloids Surf. A*, 2013, 420, 89.
- [38] J. Cao, B. D. Luo, H. L. Lin, B. Y. Xu, S. F. Chen, *J. Hazard. Mater*, 2012, 217, 107.
- [39] M. A. Butler, *Journal of Applied Physics*, 1977, 48, 1914.
- [40] H. Xua, H. M. Li, G. S. Sun, J. X. Xia, C. Wu, Z. X. Ye, Q. Zhang, *Chem.Eng. J.*, 2010, 160, 33.
- [41] M. J. Zhou, X. L. Liu, C. C. Ma, H. Q. Wang, Y. F. Tang, P. W. Huo, W. D. Shi, Y. S. Yan, J. H. Yang, *Appl. Catal. B*, 2015, 172, 174.
- [42] G. Li, K. H. Wong, X. Zhang, C. Hu, J. C. Yu, R.C.Y. Chan, P. K. Wong, *Chemosphere*, 2009, 76, 1185.
- [43] S. Q. Liu, N. Zhang, Z. R. Tang, Y. J. Xu, *ACS Appl. Mater. Interfaces*, 2012, 4, 6378.
- [44] S. C. Yan, Z. S. Li, Z. G. Zou, *Langmuir*, 2010, 26, 3894.
- [45] U. A. Joshi, J. R. Darwent, H.H.P. Yiu, M. J. Rosseinsky, *J. Chem. Technol. Biotechnol*, 2011, 86, 1018.
- [46] S. M. Wang, D. L. Li, C. Sun, S. G. Yang, Y. Guan, H. He. *Appl. Catal. B*, 2014, 144, 885.
- [47] J. Kim, C. W. Lee, W. Choi, *Environ. Sci. Technol*, 2010, 44, 6849.
- [48] L. S. Zhang, K. H. Wong, H. Y. Yip, C. Hu, J. C. Yu, C. Y. Chan, P. K. Wong, *Environ. Sci. Technol*, 2010, 44, 1392.

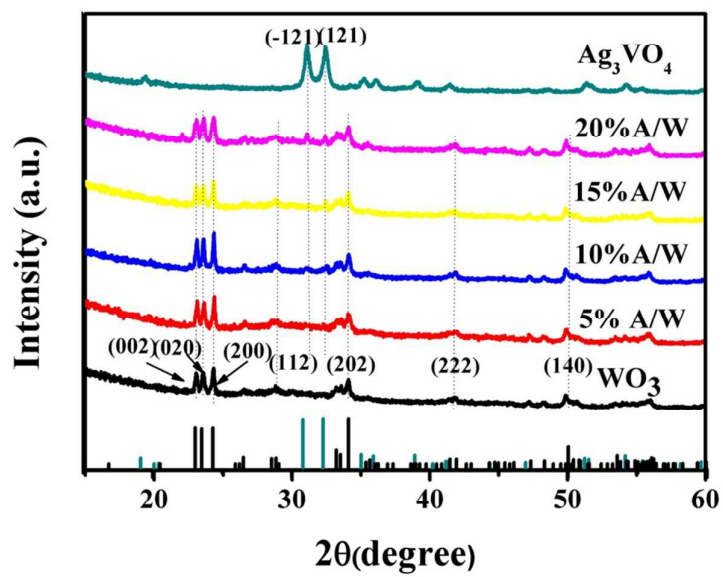


Fig.1. XRD patterns of the as-prepared samples.

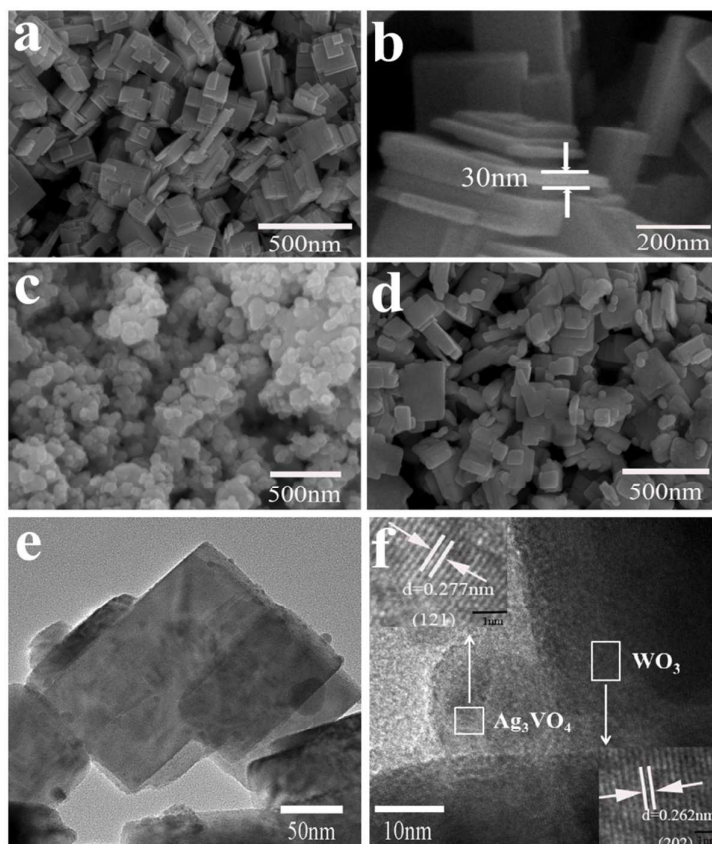


Fig.2. SEM images of prepared samples WO₃ (a-b), Ag₃VO₄ (c), 10%A/W (d), TEM (e) and HRTEM (f) images of 10%A/W

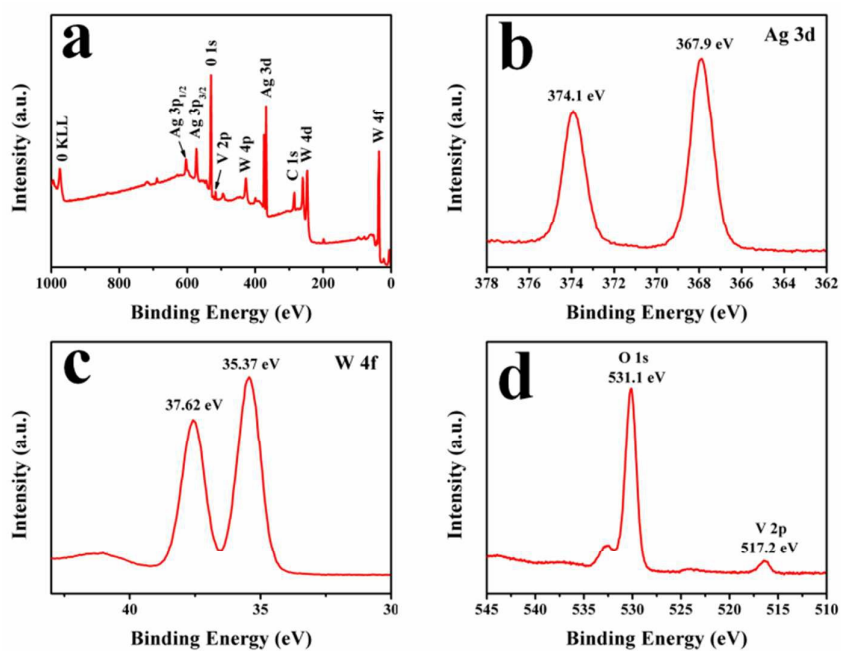


Fig.3. Survey XPS spectra (a), high-resolution XPS spectrum of Ag (b), W (c), O and V (d).

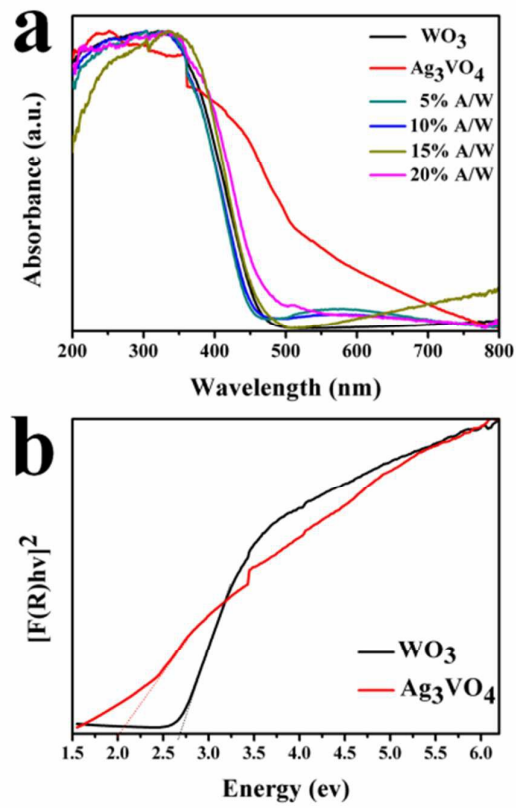


Fig.4. UV-vis adsorption spectra with as-prepared samples (a), calculated band gap of WO₃ and Ag₃VO₄ (b).

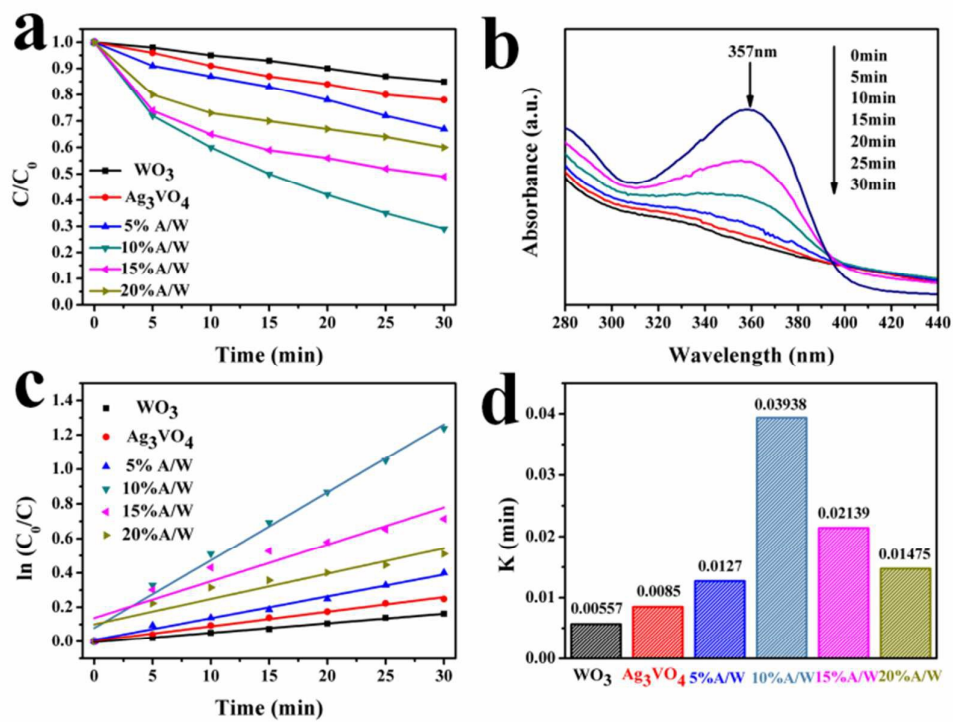


Fig.5. Photocatalytic degradation of TC with as-prepared samples (a); Time-dependent UV-vis absorption spectra of the TC solution in the presence of 10%A/W sample (b); The pseudo-first-order reaction kinetics for TC degradation (c); The apparent rate constants for TC degradation (d).

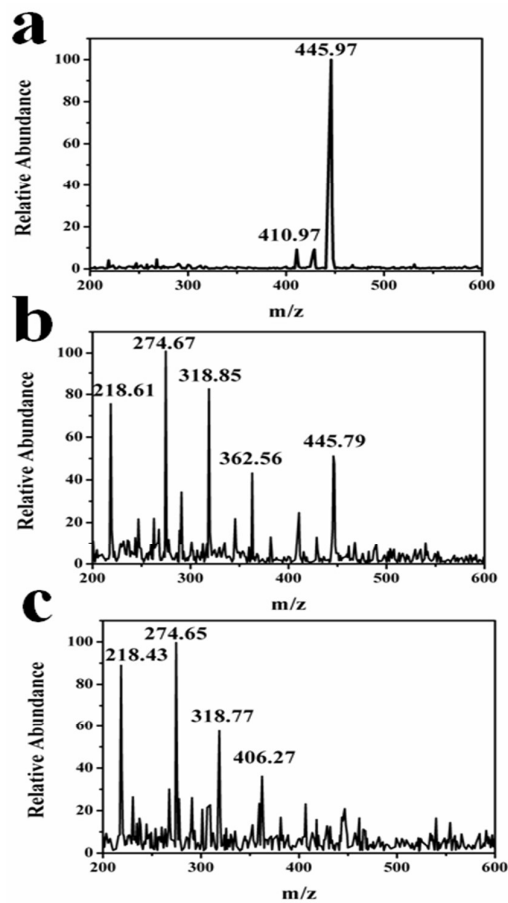


Fig. 6. Typical LC–MS chromatogram and m/z of degraded tetracycline (a) tetracycline, (b) degradation of tetracycline in 15 min, and (c) degradation of tetracycline in 30 min.

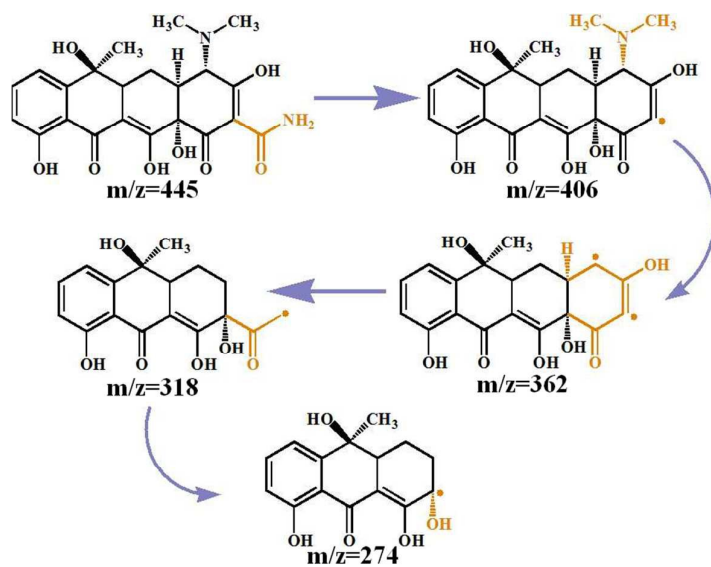


Fig. 7. Proposed degradation pathways for photocatalytic degradation of TC with 10%A/W sample.

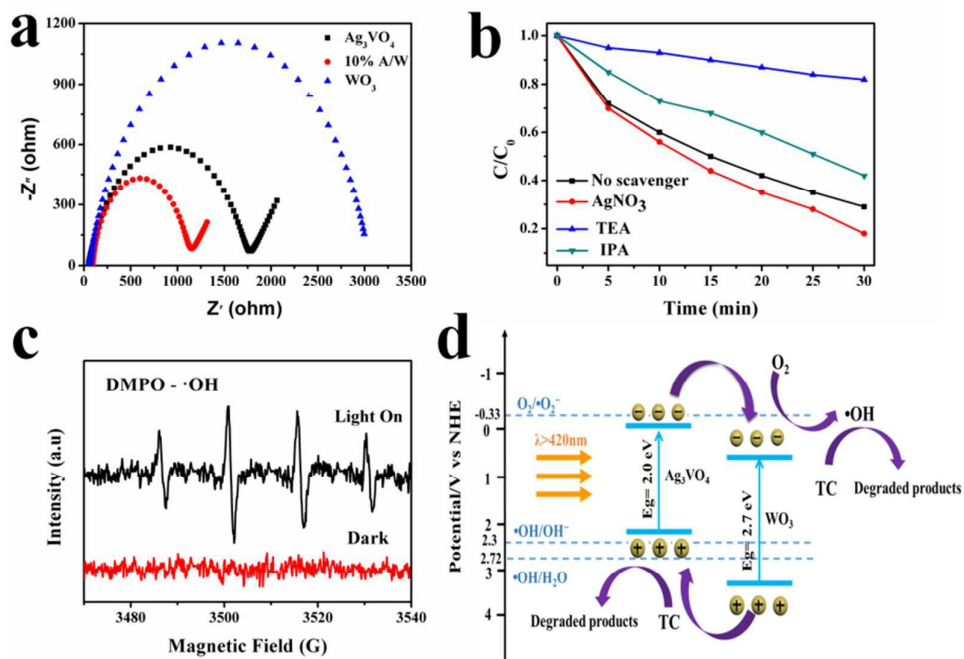


Fig.8. (a) EIS for the WO_3 , Ag_3VO_4 and 10%A/W samples; (b) photocatalytic degradation ratios of TC using different radical scavengers over 10%A/W sample; (c) DMPO spin-trapping ESR spectra; (d) the possible photocatalytic mechanism.